THE FOUR POINT SHEAR TEST ON SINGLE NOTCHED SPECIMENS: AN EXPERIMENTAL AND NUMERICAL ANALYSIS.

Alberto Carpinteri *
Gerardo Ferrara **
Giorgio Melchiorri **
Silvio Valente *

An experimental and numerical investigation is carried out for a particular testing geometry: the single edge notched specimen subjected to four point shear, where a Mixed Mode crack propagation is activated in concrete, if the specimen is not too small and the aggregates are not too large. When both such conditions are verified, each crack growth step is governed locally by a Mode I strain field and the energy dissipation is tendentially provided by the fracture energy G_F, whereas permanent deformation in the bulk material and interlocking on the crack surface, result to be negligible.

INTRODUCTION

The single edge notched specimen subjected to four point shear, firstly proposed in (1) for concrete, was then reproposed in (2-5) with two symmetrical initial cracks- the so-called double edge notched specimen subjected to four point shear. Purpose of these studies was analyzing the different failure mechanisms involved by varying geometrical ratios and size-scale of the specimen. The Mixed Mode crack propagation is thus in competition with other two failure mechanisms:
(1) the bending failure at the supports;
(2) the splitting failure at the specimen center.

With large-sizes, Mixed Mode crack propagation is favoured and prevails over the two strength overcoming mechanisms. Even with small aggregates, Mixed Mode crack propagation prevails and the energy dissipation is confined to the crack surface. In both cases, Mixed Mode

* Politecnico di Torino, Dept. of Structural Engineering, 10129 Torino, Italy
**ENEL-CRIS, 20162 Milano, Italy

fracture energy and Mode I fracture energy G_F result to be very close, since the additional energy dissipation by permanent deformation in the bulk material, as well as by friction and interlocking, tends to be negligible.

MATERIAL PROPERTIES AND EXPERIMENTAL PROGRAM

Two different concretes, with maximum aggregate size D_{max} = 10 and 20mm respectively, were selected to extend the experimental program published in (6).

Three point bending tests were carried out to obtain the fracture energy G_F according to the RILEM Recommandation (7). The same fracture toughness parameter was determined also by stable direct tension tests on prenotched cylindrical specimens of diameter Φ = 10cm and height H = 20cm. The related experimental results, averaged over four identical specimens, are reported in Table 1.

TABLE 1: Mode I Fracture energy G_F

Testing procedure	Specimen sizes	Concrete	Fracture energy G_F (N/m)
Stable three-point bending test	10·10·84 cm	1 2	116.7 ± 12.4 117.8 ± 19.9
Stable tension test	ϕ - 10 H - 20	1 2	125.7 ± 7.3 124.2

Four identical single edge notched shear specimens (Fig.1) were tested for each case of Table 2. The specimens were kept in a controlled environment at 20°C and 95% relative humidity up to four hours before testing. The notches were performed by means of a circular saw. Each specimen was provided with four steel supports of sizes 2x2x10 cm, glued at the four intended loading points, and with displacement transducers (LVDT) to measure the following quantities (6).

- Two transducers to measure the deflections δ_1 and δ_2 of the two upper loading points.
- Two transducers (one per each side of the beam) to measure the crack mouth sliding displacement (CMSD).

- One central transducer to measure the crack mouth opening displacement (CMOD).

TABLE 2: Testing geometries

Concrete	D max (mm)	Specimen	Thickness t (cm)	Depth b (cm)	Length L (cm)	Span l (cm)	Crack length a (cm)	Support distance c (cm)
1	10	1 B	10	20	84	80	4	8
		1 C	10	30	125	120	6	12
2	20	2 C	10	30	125	120	6	12

The tests were carried out using a servocontrolled machine (max.load=60t) and the deflection δ_2 as feed-back signal (6). The imposed deflection rate was appoximately 0.025 μm/sec.

The following diagrams were recorded.

- P vs δ_1 and P vs δ_2, P being the total load, from which it is possible to obtain the curves F_1 vs δ_1 and F_2 vs δ_2, for the evaluation of the Mixed Mode fracture energy (Fig.2).

- P vs CMSD, where CMSD is the average between the two transducers on the two beam sides, in order to take into account torsional effects.

- P vs CMOD.

The results are displayed in Table 3, for concrete 1 and 2 respectively. Mixed Mode fracture energy is defined as the ratio of total dissipated energy to total fracture area. Mixed Mode fracture energy results to be higher than Mode I fracture energy, ~19% with small aggregates (specimen 1C) and ~33% with large aggregates (specimen 2C), the specimen depth being equal to 30 cm. This is very likely due to additional energy dissipation by interlocking, which is higher with larger aggregates. On the other hand, the increase is ~19% with large specimens (1C) and ~31% with small specimens (1B), for concrete 1. The interlocking effect appears to increase with decreasing specimen size.

The same trends were found in the preceding experimental investigation (6).

NUMERICAL SIMULATION

The experimental tests were simulated by a finite element procedure, where the controlling parameter is the crack length (8-10). For mixed mode non-collinear crack propagation a continuous modification of the mesh is required. A finite element rosette is roto-translated at each crack growth step. Fig.3 shows three different steps of the crack propagation process in specimen 2C. The presence of cohesive strain-softening forces is indicated by the connections. At the first step the cohesive zone is missing and the load P producing the ultimate tensile stress at the crack tip is computed. Such a value, P, together with the related loading point displacement, δ, gives the first point of the P vs δ diagram. The fictitious crack tip propagates by a pre-defined length Δa in a direction orthogonal to the maximum circumferential stress (11). Then, the load P producing the ultimate tensile stress at the up-dated fictitious crack tip and the related deflection δ are computed at each step in order to obtain the subsequent points of the diagram.

The substructures used in the numerical simulation are shown in Fig.4, whereas the deformed configurations at the computation steps 6, 14 and 26, are represented in Fig.5, with a magnification factor equal to 300. The material properties assumed in the numerical analysis are the following:

Young's modulus, $E = 40{,}000$ MPa
Poisson ratio, $\nu = 0.1$
Ultimate tensile stress, $\sigma_u = 2$ MPa
Fracture energy, $G_F = 125$ N/m

It is worthwhile to remark that the propagation of the real crack tip begins only at the step 29, when the uncracked ligament is less than 1/5 of the beam depth.

The numerical load vs deflection diagrams, F_1 vs δ_1 and F_2 vs δ_2, are reported in Fig.2, together with the experimental ones, averaged over four specimens. The loading point 1 (Fig.1) undergoes a quasi-elastic unloading with small permanent deformation, while the loading point 2 undergoes a softening unloading with ever increasing deformation.

ACKNOWLEDGEMENTS

The present preliminary results were obtained in a joint research program between ENEL-CRIS-Milano and Politecnico di Torino.

REFERENCES

(1) Arrea, M. and Ingraffea, A.R., "Mixed mode crack propagation in mortar and concrete", Department of Structural Engineering, Cornell University, Report 81 - 13, 1981.

(2) Ingraffea, A.R. and Panthaki, M.J., "Analysis of shear fracture tests of concrete beams", Seminar on Finite Element Analysis of Reinforced Concrete Structures, May 21 - 24, 1985, Tokyo, pp.71-91.

(3) Bazant, Z.P. and Pfeiffer, P.A., "Shear fracture tests of concrete", Materials & Structures, Vol.19, 1986, pp.111-121.

(4) Ballatore, E., Carpinteri, A., Ferrara, G. and Melchiorri, G., "Mixed mode fracture energy of concrete", Engineering Fracture Mechanics, Vol.35, N°1/2/3, 1990, pp.145-157.

(5) Bocca, P., Carpinteri, A. and Valente, S., "Size effects in the mixed mode crack propagation: softening and snap-back analysis", Engineering Fracture Mechanics, Vol.35, N°1/2/3, 1990, pp.159-170.

(6) Carpinteri, A., Ferrara, G. and Melchiorri, G., "Single edge notched specimen subjected to four point shear: an experimental investigation", Int. Conf. on Recent Developments in the Fractures of Concrete and Rock, Edited by S.P. Shah, S.E. Swartz, B. Barr, Elsevier Applied Science, Cardiff, England, 1989, pp.605-614.

(7) R.I.L.E.M. Recommendation "Determination of the fracture energy of mortar and concrete by means of three point bend tests on notched beams", Materials & Structures, Vol.18, 1985, pp. 287-290.

(8) Carpinteri, A. and Valente, S., "Size-scale transition from ductile to brittle failure: a dimensional analysis approach", CNRS-NSF Workshop on Strain Localization and Size Effect due to

Cracking and Damage, Edited by Z.P. Bažant, J. Mazars, Elsevier Applied Science, Cachan, France, 1988, pp.477-490.

(9) Carpinteri, A., Valente, S. and Bocca, P., "Mixed mode cohesive crack propagation", Seventh International Conference on Fracture (ICF7), Pergamon Press, Houston (Texas), 1989, pp.2243-2257.

(10) Bocca, P., Carpinteri A. and Valente, S., "Mixed mode fracture of concrete", Int. J. of Solids and Structures (to appear).

(11) Erdogan, F. and Sih, G.C., "On the crack extension in plates under plane loading and transverse shear", Journal of Basic Engineering, Vol.85, 1963, 519-527.

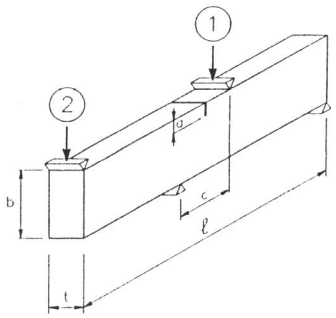

Figure 1 Single edge notched specimen subjected to four point shear.

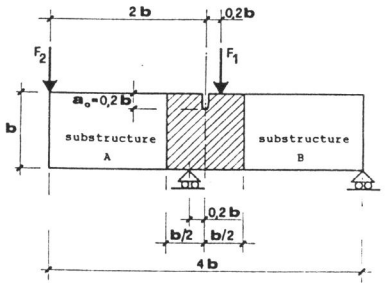

Figure 4 Substructures used in the numerical simulation.

Table 3 - Comparison between mixed-mode fracture energy and mode I fracture energy.

D_{max} (mm)	Specimen	Maximum load P (KN)	Dissipated energy Wo (N·m)	Fracture area S (m^2)	Mixed-mode fracture energy G_F^* (N/m)	Mode I fracture energy G_F (N/m)	$\frac{G_F^* - G_F}{G_F} \cdot 100$ (%)
10	1 B	56.16	2.182	0.01939	112.53	125.7	31
		69.16	3.899	0.01967	198.22		
		59.11	3.287	0.01958	167.88		
		68.18	2.826	0.02001	141.23		
					164.3 ± 51.2		
	1 C	85.35	4.769	0.02965	160.84		19
		82.89	4.727	0.03003	157.41		
		83.39	4.512	0.02893	155.96		
		79.95	3.568	0.02835	125.86		
					150.0 ± 16.2		
20	2 C	98.10	5.390	0.02830	190.46	124.2	33
		83.39	4.048	0.02847	142.18		
		93.69	5.651	0.03040	185.89		
		80.93	4.169	0.02929	142.34		
					165.2 ± 26.6		

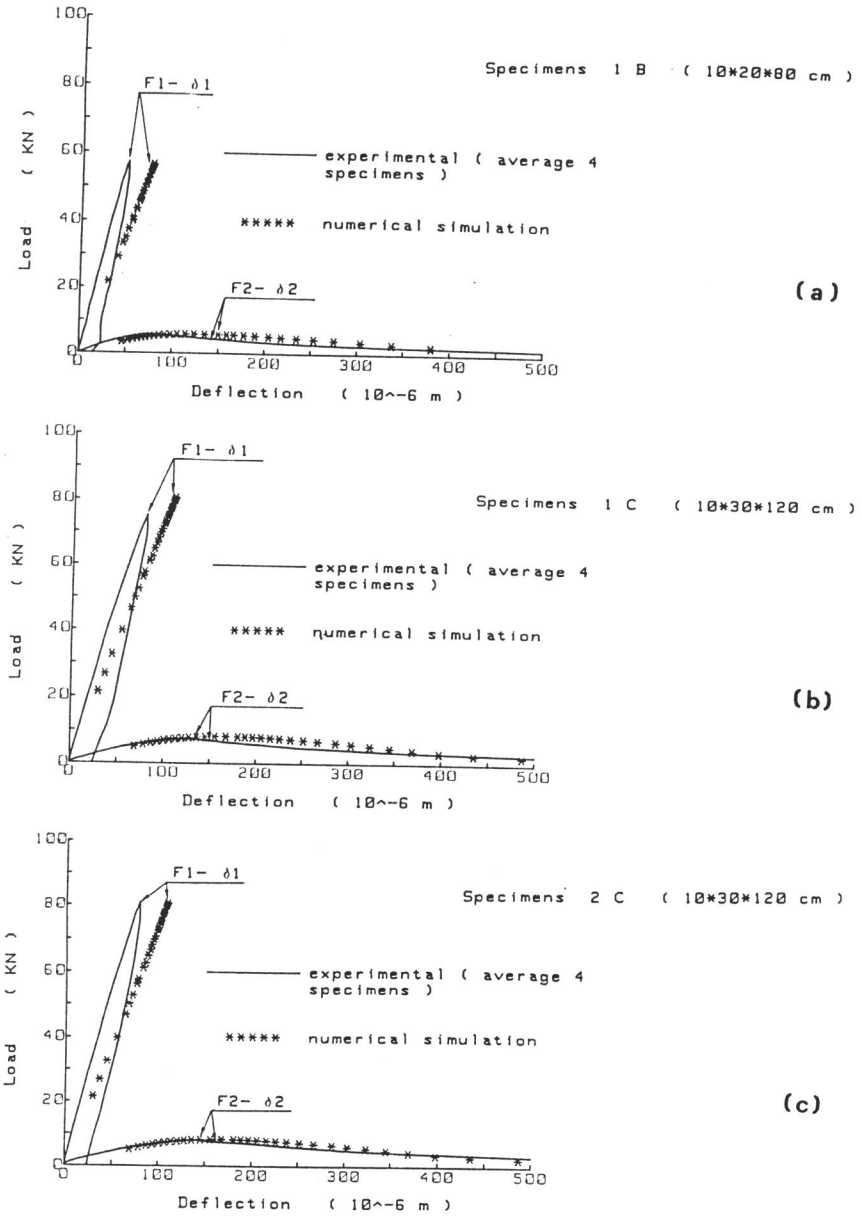

Figure 2 Experimental and numerical load vs deflection diagrams.

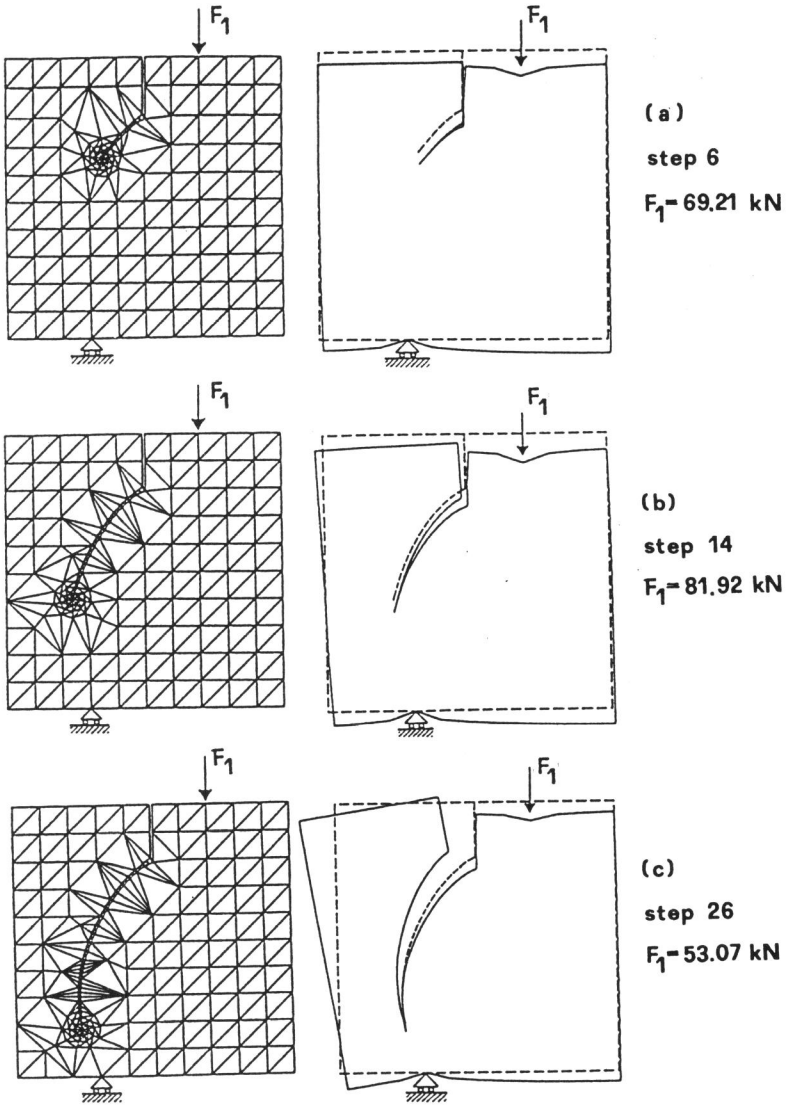

Figure 3 Finite element remeshing (specimen 2C)

Figure 5 Subsequent deformed configurations (specimen 2c)